Supporting Information

Multiple Anionic Transition-Metal Oxycarbide for Better Lithium Storage and Facilitated Multielectron Reactions

Jing Cuan,[†] You Zhou,[⊥] Jian Zhang,[#] Tengfei Zhou,[†,∥] Gemeng Liang,[†] Sean Li,[▽] Xuebin Yu,*[,§] Wei Kong Pang,[†] and Zaiping Guo*[,†,‡]

[†]Institute for Superconducting and Electronic Materials, and [‡]School of Mechanical, Materials and Mechatronics Engineering, University of Wollongong, Wollongong 2511, NSW, Australia
[§]Department of Materials Science, Fudan University, Shanghai 200433, China
[⊥]Faculty of Materials Science and Chemical Engineering, Ningbo University, Ningbo 315211, China
[#]College of Automotive and Mechanical Engineering, Changsha University of Science and Technology, Changsha 410015, China
[∥] College of Chemistry and Materials Science, South-Central University for Nationalities, Wuhan 430074, China
[▽]School of Materials Science and Engineering, University of New South Wales, Sydney 2052, Australia

Experimental Section

Synthesis of MoOC/MoO_2*-NCNW and bulk MoOC/*MoO_2 1 mmol ammonium molybdate and 18 mmol aniline were dispersed in 20 ml deionized water at 30 °C, and then dilute hydrochloric acid was added into the above solution and the pH was adjusted until a pale-yellow viscous precipitate emerged. Then, the mixed solution was heated at 50 °C for 3 h until a custard-like precipitate formed. Centrifugal separation of the Mo-nanowire precursor precipitate was conducted at 11000 rpm, and it was washed with ethanol at least 3 times. The samples were dried in air at 50 °C for 24 h. Finally, MoOC/MoO_2-NCNW and bulk MoOC/MoO_2 were obtained by calcining the precipitate of Mo-nanowire precursor and ammonium molybdate in individual corundum crucibles at 700 °C for 3 h under slow flowing Ar gas.

Synthesis of MoO_2*-NCNW and bulk* MoO_2 1 mmol ammonium molybdate and 18 mmol aniline were dispersed in 20 ml deionized water at 30 °C, and then dilute hydrochloride acid was added into the above solution, and then the pH was adjusted until a pale-yellow viscous precipitate emerged. The mixed solution was then heated at 50 °C for 3 h until a custard-like precipitate formed. Centrifugal separation of the precipitate was conducted at 11000 rpm, and it was washed with ethanol at least 3 times. The samples were dried in air at 50 °C for 24 h. Finally, MoO_2-NCNW and bulk MoO_2 were obtained by calcining the Mo-nanowire precursor and ammonium molybdate in individual corundum crucibles at 700 °C for 3 h under fast flowing Ar gas.

Materials characterization

The crystalline structure, phase purity and composition of the products were examined with a GBC MMA X-ray diffractometer with Cu Kα radiation at a scanning rate of 2° min^{-1}. The XRD data was analyzed using GSAS-II.[1] Raman spectra of all the samples were recorded using a JobinYvon HR800 Raman spectrometer. The particle size and morphologies of the as-collected samples were characterized by field emission scanning electron microscopy (FESEM, JEOL JSM-7500FA). The scanning transmission electron microscope (STEM, JEOL JEM-ARM200F) was set to 200 kV and employed to investigate the detailed crystal structure and provide energy dispersive spectroscopy (EDS) mapping of the products. X-ray photoelectron spectroscopy (XPS) plots were recorded on a VG Multilab 2000 (VG Inc.) photoelectron spectrometer employing monochromatic Al Kα radiation under vacuum at 2×10^{-6} Pa. Continuous-wave electron paramagnetic resonance (EPR) experiments were conducted by a Bruker ELEXSYS E580 spectrometer operating in the X-band (9.4 GHz) mode and equipped with an Oxford CF935 helium flow cryostat with an ITC-5025 temperature controller.

Electrochemical measurements

CR2032 coin-type cells and Celgard separators were used in all electrochemical performance testing, employing lithium metal as counter/reference electrode. Both the cyclic voltammetry profiles and electrochemical impedance spectra were recorded on a VMP-3 electrochemical workstation using a scan rate of 0.1 $mV \cdot s^{-1}$. The cells were discharged/charged galvanostatically on a Land CT2001A battery tester at different current densities within the voltage range of 0.05–3.0 V *versus* Li^+/Li. Galvanostatic intermittent titration technique (GITT) tests were also conducted on this apparatus at room temperature in the voltage range of 0.05–3.0 V. A Bitrode unit was programmed to supply a constant current flux (C/10) for 20 min to the cell followed by standing at open circuit for 120 min. The slurries of the working electrodes were prepared through homogeneously mixing the as-synthesized materials, sodium carboxymethyl cellulose, and Super P according to a weight ratio of 80:10:10. The resultant slurries were pasted on Cu foil, vacuum-dried at 80 °C for 12 h, and then pressed at 300 $kg \cdot cm^{-2}$. The material mass loading on the individual electrodes was around 1.0 $mg \cdot cm^{-2}$. The electrolyte consisted of 1 M $LiPF_6$ in ethylene carbonate/diethyl carbonate/ dimethyl carbonate (volumetric ratio of 1:1:1).

In-situ synchrotron X-ray powder diffraction (SXRPD) of $MoOC/MoO_2$

The *in-situ* synchrotron X-ray powder diffraction patterns of bulk $MoOC/MoO_2$ anode were collected with a MYTHEN microstrip detector at the wavelength of 0.688273 Å (determined using a LaB6 NIST SRM 660b) during charging and discharging processes, considering its high crystallinity. The range from 11 to 19° can cover the diffraction peaks and clearly exhibit the structural evolution of MoO_2 and MoOC. The measurements were carried out at the Powder Diffraction Beamline, Australian Synchrotron. The testing cell employed similar coin cells components to those used in the electrochemical performance testing, which contains the counter/reference lithium metal electrode, the working electrode, and Celgard separator. The testing cell was cycled galvanostatically (equivalent to a constant current of ~ 100 mA/g) within the potential window of 0.05-3.0 V (*vs.* Li^+/Li), using a customized CR2032 coin cell. The detailed information has been shown elsewhere.[2] The lattice evolution and changes in peak position, intensity, and width of $MoOC/MoO_2$ during lithiation/delithiation were examined using single - peak-fitting analysis with the Large-Array Manipulation Program (LAMP).[3]

DFT calculations

All Density-Functional-Theory (DFT) calculations were conducted using the DMol[3] software package.[4] The PBE [5] exchange-correlation functional was adopted for generalized gradient approximation (GGA) correction.[6] All-electron Kohn-Sham wave functions were expanded in a double numerical plus d-functions (DND) basis.[7] The sampling of irreducible wedge of Brillouin zone was performed with a regular Monkhorst-Pack grid of special k-points.[8] The

convergences criteria of relaxation were 2.0×10^{-5} Ha, 0.004 Ha/ Å and 0.005 Å for energy, gradient and atomic displacement, respectively. For the MoOC crystals, the structure was optimized in a cubic cell (space group *Fm/3m*) with lattice parameters of a = 4.1587Å, b = 4.1587 Å, c = 4.1587 Å and $\alpha = \beta = \gamma = 90°$. For the MoO_2 crystals, the structure was optimized in a monoclinic cell (space group *P21/c*) with lattice parameters of a = 5.6289 Å, b = 4.8696 Å, c = 5.6222 Å and $\alpha = \gamma = 90°$, $\beta = 120.4446^{o}$.

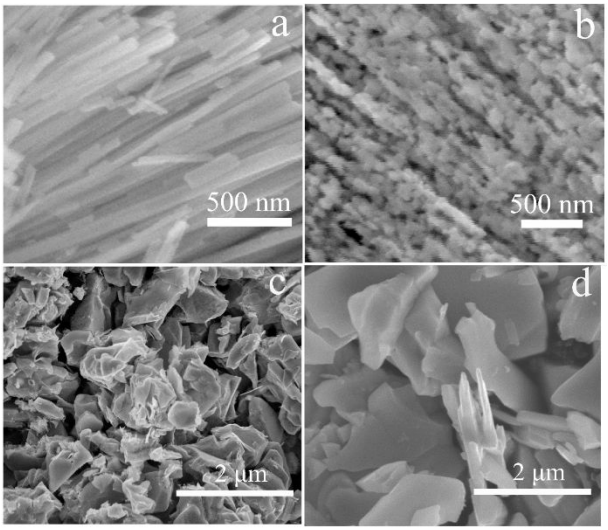

Figure S1. (a) SEM image of $Mo_3O_{10}(C_6H_8N)_2 \cdot 2H_2O$ nanowire precursor. (b) SEM image of MoO_2-NCNW. (c) SEM image of bulk MoO_2. (d) SEM image of bulk MoOC/MoO_2.

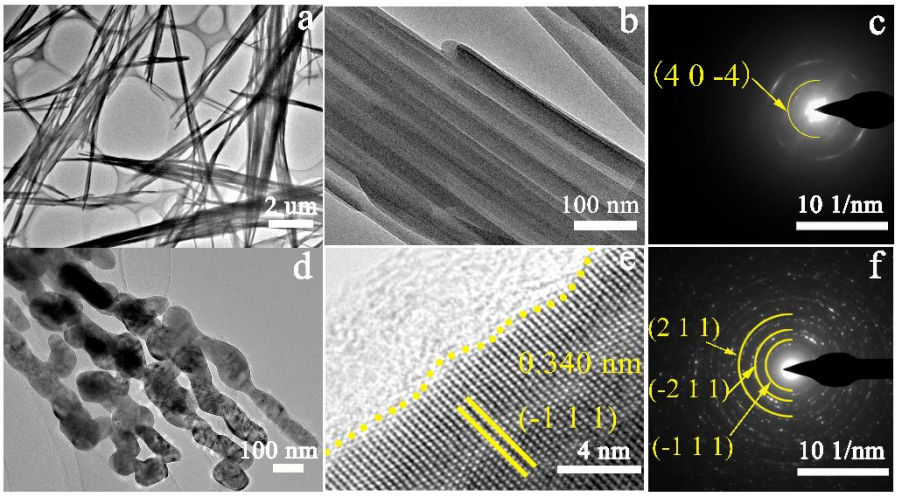

Figure S2. (a-c) TEM images and selected-area electron diffraction (SAED) pattern of $Mo_3O_{10}(C_6H_8N)_2 \cdot 2H_2O$. (d-f) TEM images and selected-area electron diffraction (SAED) pattern of MoO_2-NCNW.

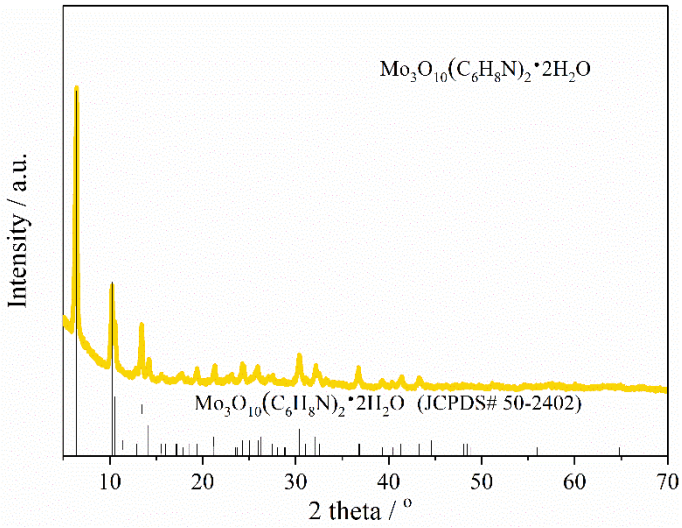

Figure S3. XRD pattern of $Mo_3O_{10}(C_6H_8N)_2{\cdot}2H_2O$ nanowire precursor.

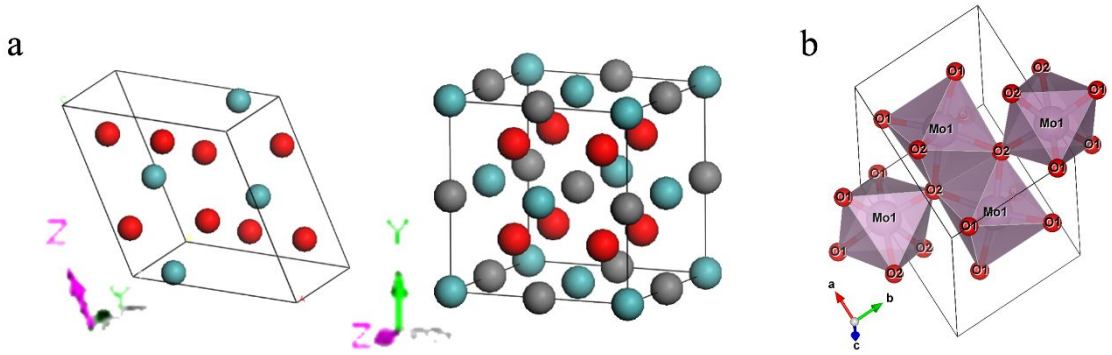

Figure S4. Crystal structures of (a) monoclinic MoO_2 (left) and cubic MoOC (right). Red balls: O atoms. Green balls: Mo atoms. Grey balls: C atoms. (b**)** The crystal structure of MoO_2 phase, revealing two types of coordinating oxygen sites.

Table S1. Crystallographic details of the as-prepared samples.

MoOC				
Cubic, Space group: *Fm-3m*		lattice parameters: $a = b = c = 4.1587(2)$ Å		
Atom	*x*	*y*	*z*	Site occupancy factor
Mo	0	0	0	1
C	0.5	0.5	0.5	0.25
O	0.5	0.5	0.5	0.25

MoO_2				
Monoclinic, Space group: *P21/c*			lattice parameters: *a = 5.62891 Å, b = 4.86957 Å, c = 5.62220 Å and α = γ = 90°, β = 120.4446°.*	
Atom	*x*	*y*	*z*	Site occupancy factor
Mo	0.22764	1.02855	0.00648	1
O1	0.07962	0.25986	0.20389	1
O2	0.49136	0.74242	0.12053	1

Table S2. Comparison of lattice constants and Mo-O bond length between pristine MoO_2, MoO_2 reported in previous work, and MoO_2 phase in MoOC/MoO_2 composite. Unit: Angstrom

Crystal Lattice Parameters	**Pritine MoO_2**	**Previous work[9]**	**MoO_2 in MoOC/MoO_2**
a	5.610	5.610	5.629
b	4.856	4.843	4.870
c	5.628	5.526	5.622
$d_{\text{Mo-O (1)}}$	1.973	1.961	1.799
$d_{\text{Mo-O (1)}'}$	1.984	1.923	2.031
$d_{\text{Mo-O (1)}''}$	1.995	1.975	2.071
$d_{\text{Mo-O (2)}}$	2.063	2.106	2.151
$d_{\text{Mo-O (2)}'}$	1.979	2.011	1.891
$d_{\text{Mo-O (2)}''}$	2.072	2.033	2.542
Average $d_{\text{Mo-O}}$	2.011	2.002	2.080

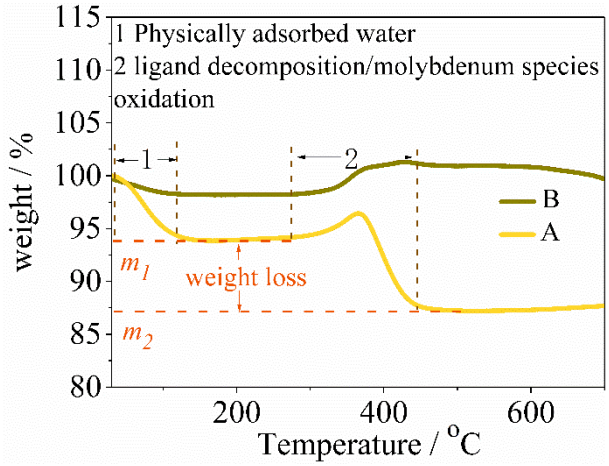

Figure S5. TGA profiles of MoOC/MoO_2-NCNW (A) and MoO_2-NCNW (B) tested under air atmosphere with a heating rate of 5 $^oC \cdot min^{-1}$.

Table S3. Weight ratio of carbon, MoO_2, and MoOC.

Sample	$MoOC_{\text{weight ratio}}$/ %	$MoO_{2\text{weight ratio}}$/ %	$C_{weight\ ratio}$/ %
MoOC/MoO_2-NCNW	13.2	69.1	17.7
MoO_2-NCNW	0	89.7	10.3

Supplementary Note 1. Calculation of the carbon content ($C_{\text{weight ratio}}$) of the MoOC/MoO_2-NCNW sample has been taken as an example, according to the combined results of the Rietveld analysis (**Figure 2c**) and TGA data (**Figure S5**). The refinement analysis indicates that the MoOC/MoO_2-NCNW sample consists of 11(4) wt.% MoOC and 89(4) wt.% MoO_2.

m_1 represents the weight ratio of the dry MoOC/MoO_2-NCNW composite, and m_2 represents the weight ratio of the final product (MoO_3) after TGA analysis (**Figure S5**). We suppose that: y is the mass of carbon in MoOC/MoO_2-NCNW, x is the mole number of the MoOC component, and ax is the mole number of the MoO_2 component (with a calculated from **Figure 2c**).

$$C + \text{MoOC} + \text{MoO}_2 \rightarrow \text{MoO}_3$$

$$y \qquad 124x \qquad 128ax \qquad 144(1+a)x$$

$$(124x+128ax+y)/(144(1+a)x)=m_1/m_2$$

In MoOC/MoO_2-NCNW sample, since a is 5.1, Solution 1: $y = 166.7x$

$$since\ C_{(weight\ ratio)}=y/(124x+128ax+y)$$

Thus, the $C_{\text{weight ratio}}$ of the MoOC/MoO_2-NCNW sample is 17.7 %.

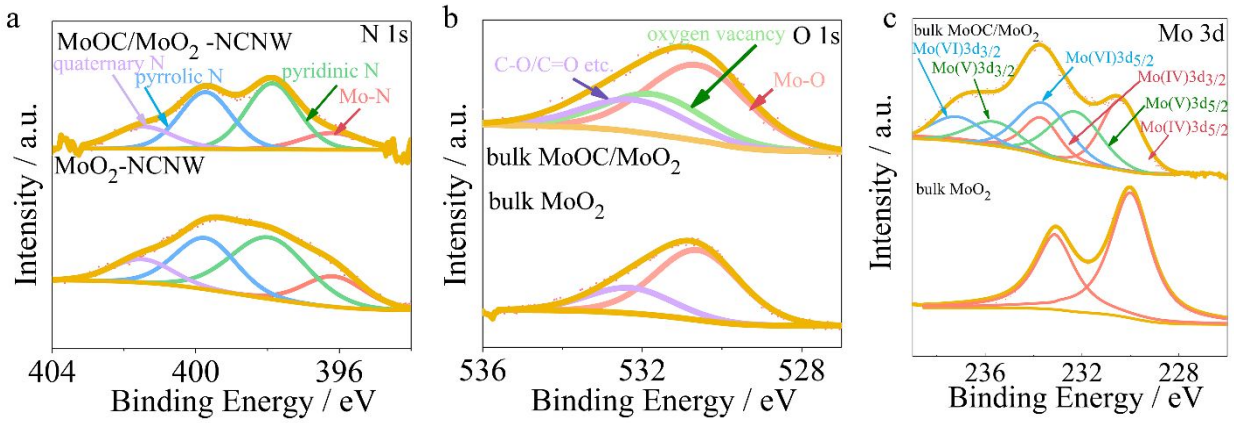

Figure S6. (a) N 1s high resolution XPS spectra of MoO_2-NCNW and MoOC/MoO_2-NCNW. (b) O 1s high resolution XPS spectra of bulk MoO_2 and bulk MoOC/MoO_2, (c) Mo 3d high resolution XPS spectra of bulk MoO_2 and bulk MoOC/MoO_2.

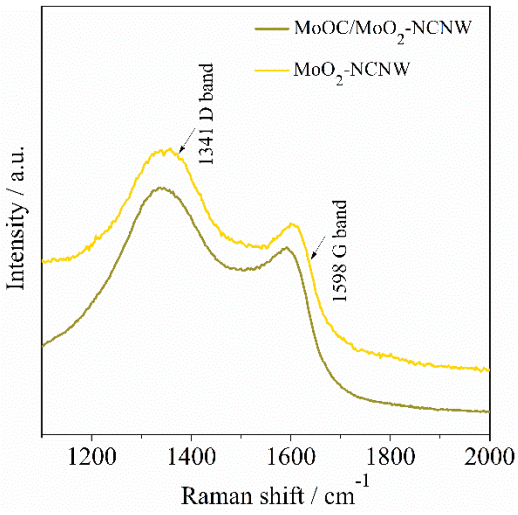

Figure S7. Raman spectra of MoOC/MoO_2-NCNW and MoO_2-NCNW within the range of 1100 - 2000 cm^{-1}.

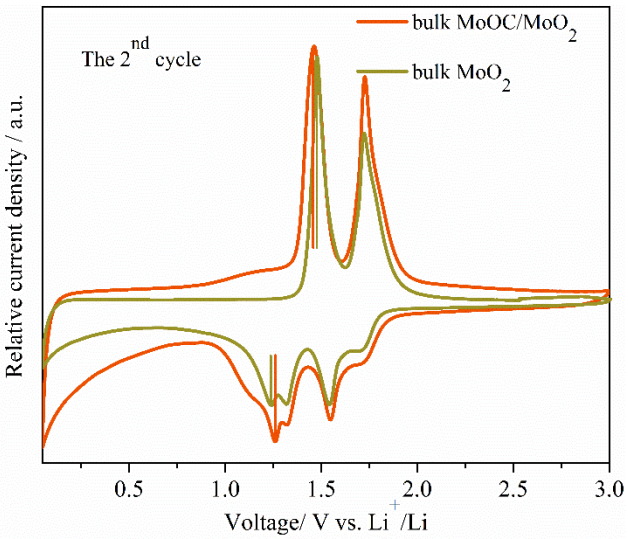

Figure S8. Cyclic voltammetry profiles of bulk $MoOC/MoO_2$ and bulk MoO_2.

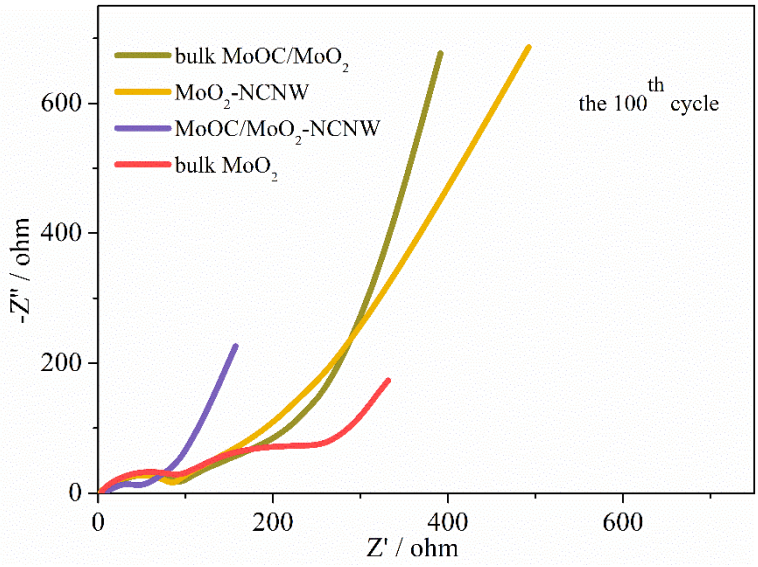

Figure S9. Electrochemical impedance spectra of the as-collected samples tested after 100 cycles (fully discharged down to 0.05 V) at 1000 mA·g^{-1}.

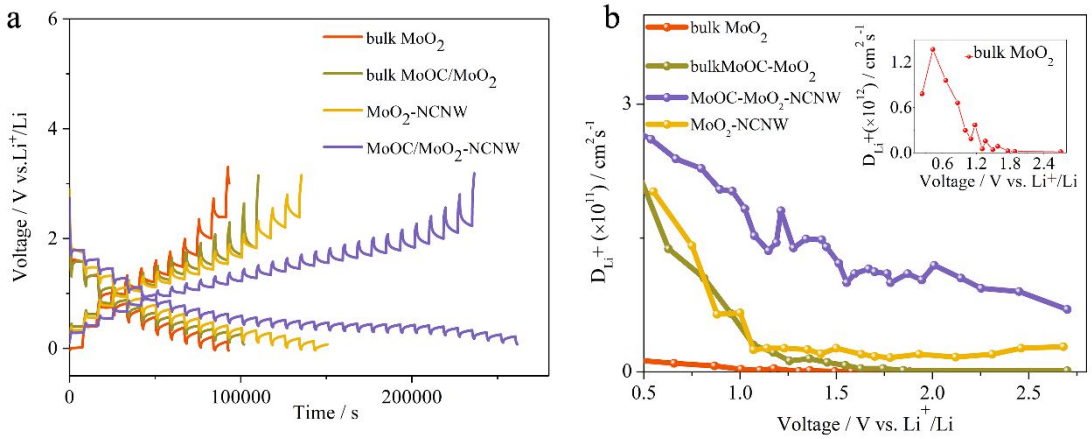

Figure S10. (a) Galvanostatic intermittent titration technique (GITT) profiles of the as-collected samples. (b) The plots of the lithium chemical diffusion coefficients for the samples in the discharged state obtained by GITT as a function of potential. The inset is an enlargement of the curve for bulk MoO_2.

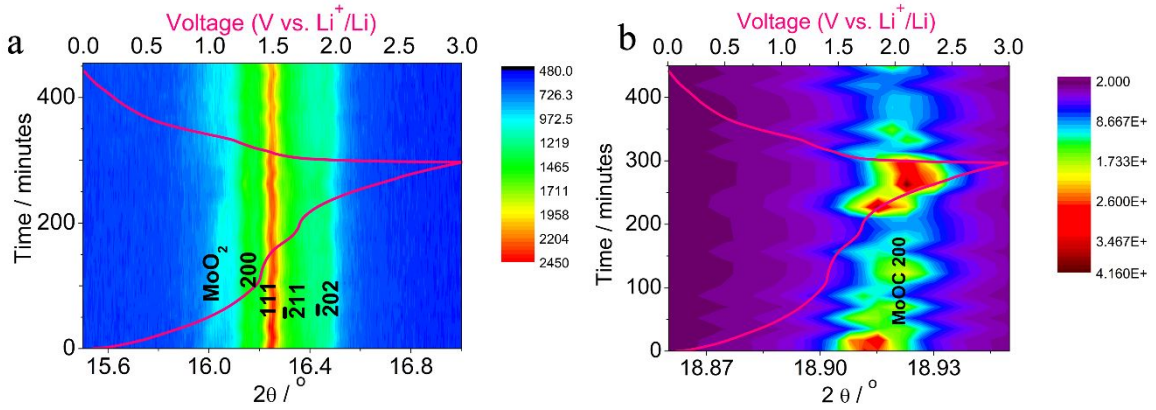

Figure S11. Contour plots based on operando synchrotron X-ray powder diffraction data for bulk MoOC/MoO_2, collected during electrochemical cycling, with the charge-discharge profile superimposed. They show the variation of typical (200), (111)/($\bar{2}$11), and ($\bar{2}$02) diffraction peaks of MoO_2 phase (a) and the (200) diffraction reflections of MoOC phase (b) of bulk MoOC/MoO_2. These positions did not move significantly during the cycling process, suggesting that the lattice parameters remained nearly unchanged during the electrochemical reactions.

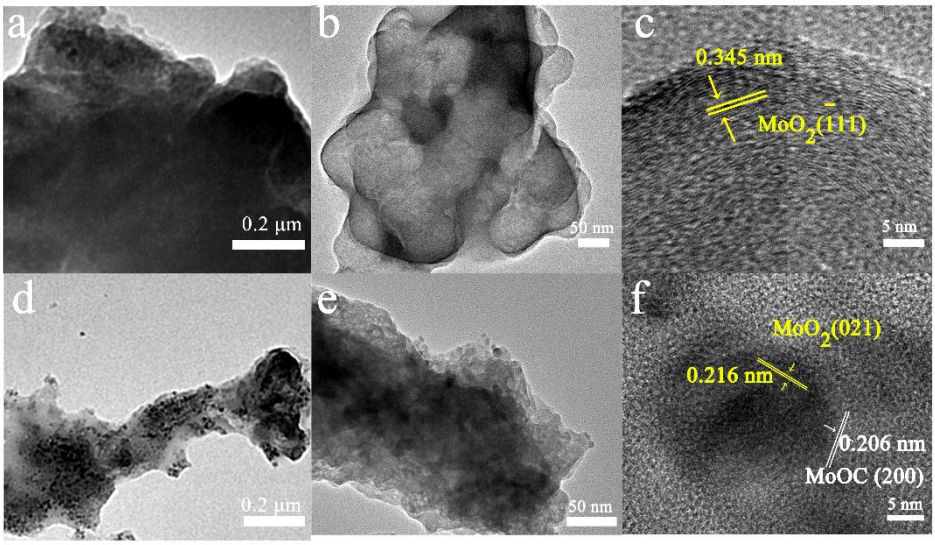

Figure S12. TEM images of (a-c) MoO_2-NCNW and (d-f) MoOC/MoO_2-NCNW samples after 100 cycles at 100 $mA \cdot g^{-1}$.

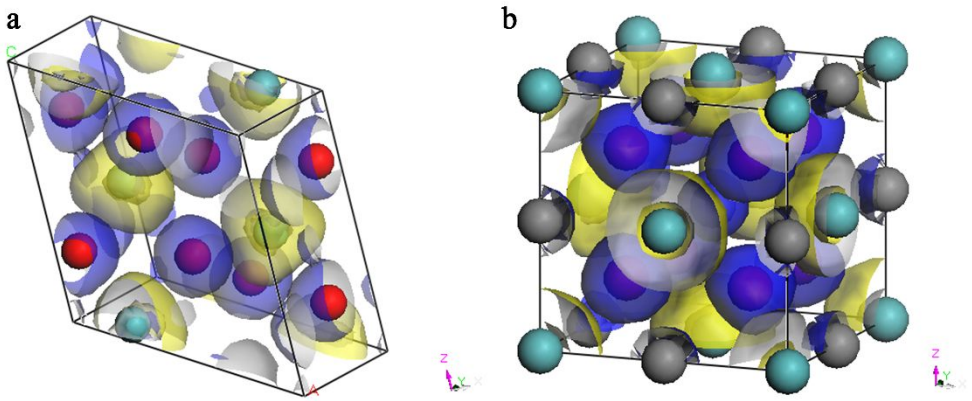

Figure S13. Comparison of charge distribution around Mo atoms of MoO_2 and MoOC compound simulated based on first-principles DFT calculations: a) monoclinic MoO_2 phase, b) cubic MoOC phase. Red balls: O atoms. Green balls: Mo atoms. Grey balls: C atoms. The yellow and blue colors of electronic density in Figure S13a, b indicate decrease and increase of the charge density, respectively.

References

1. Toby, B. H.; Von Dreele, R. B., GSAS-II: the Genesis of a Modern Open-Source All-Purpose Crystallography Software Package. *J. Appl. Crystallogr.* **2013**, 46, 544-549.

2. Pang, W. K.; Kalluri, S.; Peterson, V. K.; Sharma, N.; Kimpton, J.; Johannessen, B.; Liu, H. K.; Dou, S. X.; Guo, Z., Interplay between Electrochemistry and Phase Evolution of the P2-Type Na_x $(Fe_{1/2}Mn_{1/2})O_2$ Cathode for Use in Sodium-Ion Batteries. *Chem. Mater.* **2015**, 27, 3150-3158.

3. Richard, D.; Ferrand, M.; Kearley, G., Analysis and Visualisation of Neutron-Scattering Data. *J. Neutron Res.* **1996**, 4, 33-39.

4. Delley, B., From Molecules to Solids with the $DMol^3$ Approach. *J. Chem. Phys.* **2000**, 113, 7756-7764.

5. Perdew, J. P.; Burke, K.; Ernzerhof, M., Generalized Gradient Approximation Made Simple. *Phys. Rev. Lett.* **1996**, 77, 3865-3868.

6. Perdew, J. P.; Chevary, J. A.; Vosko, S. H.; Jackson, K. A.; Pederson, M. R.; Singh, D. J.; Fiolhais, C., Atoms, Molecules, Solids, and Surfaces: Applications of the Generalized Gradient Approximation for Exchange and Correlation. *Phys. Rev. B* **1992**, 46, 6671-6687.

7. Delley, B., $DMol^3$ DFT Studies: from Molecules and Molecular Environments to Surfaces and Solids. *Comput. Mater. Sci.* **2000**, 17, 122-126.

8. Monkhorst, H. J.; Pack, J. D., Special Points for Brillouin-Zone Integrations*. *Phys. Rev. B* **1976**, 13, 5188-5192.

9. Bai, L.; Zhang, Y.; Zhang, L.; Zhang, Y.; Sun, L.; Ji, N.; Li, X.; Si, H.; Zhang, Y.; Huang, H., Jahn-Teller Distortions in Molybdenum Oxides: An Achievement in Exploring High Rate Supercapacitor Applications and Robust Photocatalytic Potential. *Nano Energy* **2018**, 53, 982-992.